UNIVERSITÀ DEGLI STUDI FIRENZE

FLORE
Repository istituzionale dell'Università degli Studi di Firenze

Temperature and pH sensors based on graphenic materials

Questa è la Versione finale referata (Post print/Accepted manuscript) della seguente pubblicazione:

Original Citation:
Temperature and pH sensors based on graphenic materials / Salvo, P., Calisi, N., Melai, B., Cortigiani, B., Mannini, M., Caneschi, A., Lorenzetti, G., Paoletti, C., Lomonaco, T., Paolicchi, A., Scataglini, I., Dini, V., Romanelli, M., Fuoco, R., Di Francesco, F.. - In: BIOSENSORS & BIOELECTRONICS. - ISSN 0956-5663. - STAMPA. - 91:(2017), pp. 870-877. [10.1016/j.bios.2017.01.062]

Availability:
The webpage https://hdl.handle.net/2158/1076285 of the repository was last updated on 2021-03-31T11:41:09Z

Published version:
DOI: 10.1016/j.bios.2017.01.062

Terms of use:
Open Access
La pubblicazione è resa disponibile sotto le norme e i termini della licenza di deposito, secondo quanto stabilito dalla Policy per l'accesso aperto dell'Università degli Studi di Firenze (https://www.sba.unifi.it/upload/policy-oa-2016-1.pdf)

Publisher copyright claim:

La data sopra indicata si riferisce all'ultimo aggiornamento della scheda del Repository FloRe - The above-mentioned date refers to the last update of the record in the Institutional Repository FloRe

(Article begins on next page)

16 October 2026

Manuscript
Click here to view linked References

Temperature and pH sensors based on graphenic materials

P. Salvo[1,2,+], N. Calisi[2,+], B. Melai[2,+], B. Cortigiani[3,4], M. Mannini[3,4], A. Caneschi[3,4], G. Lorenzetti[5], C. Paoletti[2], T. Lomonaco[2], A. Paolicchi[6], I. Scataglini[6], V. Dini[7], M. Romanelli[7], R. Fuoco[2], F. Di Francesco[2,3,*]

[1] Institute of Clinical Physiology, National Council of Research (IFC-CNR), Via Moruzzi 1, 56124, Pisa, Italy.
[2] Department of Chemistry and Industrial Chemistry, University of Pisa, Via Moruzzi 13, 56124, Pisa, Italy.
[3] INSTM, National Interuniversity Consortium of Materials Science and Technology, Via G. Giusti 9, 50121 Firenze, Italy.
[4] Department of Chemistry "U. Schiff", University of Florence, Via della Lastruccia 3-13, 50019, Sesto Fiorentino (FI), Italy.
[5] Applied and Laser Spectroscopy Laboratory, ICCOM-CNR, Research Area of Pisa, Via G. Moruzzi 1, 56124 Pisa, Italy.
[6] Department of Experimental Pathology, University of Pisa Medical School, Via Roma 55, Pisa 56126, Italy.
[7] Wound Healing Research Unit, Department of Dermatology, University of Pisa, Via Roma 67, 56126 Pisa, Italy.

[+] These authors contributed equally to this work.
* Corresponding author, Email: fabio.difrancesco@unipi.it, Tel. : +39 050 2219308

Keywords: pH; temperature; graphene; flexible sensor;

Abstract

Point-of-care applications and patients' real-time monitoring outside a clinical setting would require disposable and durable sensors to provide better therapies and quality of life for patients. This paper describes the fabrication and performances of a temperature and a pH sensor on a biocompatible and wearable board for healthcare applications. The temperature sensor was based on a reduced graphene oxide (rGO) layer that changed its electrical resistivity with the temperature. When tested in a human serum sample between 25 and 43 °C, the sensor had a sensitivity of 110 ± 10 Ω/°C and an error of 0.4 ± 0.1 °C

compared with the reference value set in a thermostatic bath. The pH sensor, based on a graphene oxide (GO) sensitive layer, had a sensitivity of 40 ± 4 mV/pH in the pH range between 4 and 10. Five sensor prototypes were tested in a human serum sample over one week and the maximum deviation of the average response from reference values obtained by a glass electrode was 0.2 pH units. For biological applications, the temperature and pH sensors were successfully tested for in vitro cytotoxicity with human fibroblast cells (MRC-5) over 24 h.

1. Introduction

pH plays a critical role in regulating the reactivity of many chemical species, thus its measurement is fundamental in many fields ranging from agriculture and environmental science to chemical engineering, chemistry and food science to biology and medicine. In living organisms, metabolic processes can only take place if very specific physical and chemical conditions are met, which is why the pH of extracellular fluids, including blood plasma, is maintained at 7.4 by very efficient buffering systems. Pathologies such as diabetes, renal and respiratory failure may imbalance blood pH (American Diabetes Association, 2001; Duffin and Philipson, 2010; Kraut and Kurtz, 2005) which is why therapies require the accurate monitoring of this parameter. However, pH is also measured in other human fluids. The pH of tear fluid was shown to be significantly more acidic in contact lens wearers and more alkaline in patients with lacrimal stenosis and keratitis (Norn, 1988). Salivary pH affects dental health and can be measured during drug monitoring (Kleinberg, 1964; Mueklow et al., 1978; Osterberg et al., 1984). The pH of exhaled breath condensate is over two orders of magnitude lower than normal in patients with acute asthma and normalizes with corticosteroid therapy (Hunt et al., 2000). In urine,

changes in pH can be a sign of a metabolic syndrome or renal disease (Buckalew Jr. et al., 1968; Maalouf et al., 2007; Remer and Manz, 1995). The mild acidity of sweat, which provides partial protection from the action of certain bacteria and fungi, is related to the relatively high content of lactate and thus sweat pH carries information in relation to physical activity and body hydration levels (Coyle et al., 2010; Curto et al., 2012).

In 2010, 33 million Europeans suffered from diabetes with an impact of approximately 93 billion dollars on healthcare expenditure, and this is expected to increase (Ghimenti et al., 2013; Organisation for Economic Co-operation and Development, 2010). Diabetic patients have a 25% risk of developing a foot ulcer which often becomes infected (Singh et al., 2005). Variations in heterogeneous parameters such as temperature, pH, erythrocyte sedimentation rate and abnormal white blood count are associated with an infection (Dini et al., 2015; Eneroth et al., 1999; Salvo et al., 2015a). A local increase in temperature is associated with a high risk of developing an ulcer, thus the temperature measurement could be used for prevention (Armstrong et al., 2007). During the healing process, wounds produce exudate, which is a fluid containing water, proteins, matrix metalloproteinases (MMPs) and electrolytes (Cutting, 2009). pH measurements can be used to monitor the ulcer status since a slightly acidic wound exudate is associated with healing, whereas alkaline pH values are found in chronic or infected ulcers (Glibbery and Mani, 1992).

The literature reports many examples of temperature and pH sensors, however to the best of our knowledge there is no single wearable and biocompatible platform for the real-time monitoring of pH and temperature in direct contact with human fluids such as blood and exudate. Currently, the ulcer status and efficacy of treatment are evaluated in specialized hospital units where patients are generally examined weekly, so clinicians have no knowledge of how the ulcer is healing when the patient is at home (Warriner et al., 2012). A continuous and remote patient monitoring would provide better quality of life, personalized treatments and prompt responses in the case of infection, however at

present this is impracticable. Lavery et al. described the monitoring of ulcer temperature with a digital infrared thermometer, however this device is not for home use because it is expensive and unwearable (Lavery et al., 2007). Other wearable temperature sensors and materials reported in the literature are not yet sufficiently well developed for clinical use (Biver et al., 2015; Giuliani et al., 2014; Matzeu et al., 2012). The measurement of pH has similar limitations, as there are no wearable sensors capable of a continuous measurement at the wound site.

Within the framework of the European project SWAN-iCare, wearable temperature and pH sensors are being developed to monitor leg and diabetic foot ulcers in contact with exudate continuously over one week. Data are saved in an online database that is accessible by clinicians, who will be promptly informed if abnormal parameters are recorded (Salvo et al., 2015; Salvo et al., 2016; Texier et al., 2013; Texier et al., 2014). This paper describes the advances in the development of these SWAN-iCare sensors, which are a disposable alternative to the cumbersome and fragile glass electrode and low-accuracy paper strips.

The temperature-sensitive layer was made of reduced graphene oxide (rGO), whereas the pH-sensitive layer was made of graphene oxide (GO). Graphene is well known for its excellent properties, such as the high carrier mobility, ballistic transport, chemical robustness in aqueous environments, large surface area, and strong mechanical stiffness, which make it suitable for fast electronics and highly sensitive sensors (Akhavan et al, 2014; Lee et al., 2015). In particular, graphene-based temperature and pH sensors can lead to superior performances compared with similar alternatives in the field (Ang et al., 2008; Yang et al., 2015). The effect of temperature on the electrical resistance of few-layer graphene (FLG) and graphene nanosheets (GN) depends on the carrier scattering and shows a negative thermal coefficient with larger resistance variations associated with increasing graphene thickness (Fang et al., 2015). For GO, the sensitivity to pH depends

on the hydroxyl (OH) and carboxyl (COOH) groups, which protonate or de-protonate as the pH changes (Shih et al., 2012). The epoxy groups (COC) on the basal plane of a GO sheet can turn into hydroxyl groups at alkaline pH and partially return to their initial structure at acidic pH (Taniguchi et al., 2015). In the literature, there are several examples of how these two chemical species can be used to fabricate sensors for biomedical applications, e.g. to detect DNA sequences, leukaemia cells, metal ions, and small biomolecules such as dopamine, but not for real-time monitoring over many days (Akhavan et al., 2012a, 2014; Dong et al., 2010; Shao et al., 2010; Zhou et al., 2009). However, these approaches often require complex fabrication processes, are not suitable for real-time monitoring, and do not provide a single platform to measure both temperature and pH. In this paper, we report the fabrication, characterization and performances of rGO and GO film-based sensors for measuring temperature and pH in human serum, respectively. Our solution integrates temperature and pH sensors on the same 2D platform, with the advantages of compactness and mass production, and potential use in thin flexible electronics.

2. Experimental section

2.1 Materials

The graphite powder (14735, UCP-1 grade, Ultra “F” purity) was purchased from Alfa Aesar. For the GO and rGO synthesis, sulphuric acid (30743), potassium permanganate (13206), sodium nitrate (S5506) and ascorbic acid (A7506-1KG) were all purchased from Sigma Aldrich. The pH buffer solutions were prepared with sodium chloride (793566), citric acid monohydrate (C1909), sodium hydroxide (S8045), sodium phosphate dibasic dehydrate (71645), potassium phosphate monobasic (P9791), sodium tetraborate

decahydrate (S9640) and hydrochloric acid (84415) purchased from Sigma Aldrich. The pH and temperature sensors were designed on flexible screen-printed boards fabricated by Topflight, Italy (Fig. 1a-b). These boards consisted of a polyethylene terephthalate (PET, 125 μm thick, Coveme) substrate with silver signal tracks (5004, Loctite ECI). A polyester resin (Electrodag ML 25208, 30 μm thick, Acheson) was used to passivate the PET boards. The polydimethylsiloxane (PDMS) MED-6010 was purchased from NuSil. The PET boards had a clincher (65801-010LF, FCI) to connect to the measurement electronics.

The cell viability was assessed using the Cell Proliferation Reagent WST-1 (CELLPRO-RO Roche), the cell counting kit-8 for quantitation of the number of viable cells in proliferation and cytotoxicity assays (96992), the minimum essential medium with 2 mM L-Glutamine and 1% non-essential amino acids (MEM, 56416C), and the fetal bovine serum (FBS, F6178), which were all purchased from Sigma Aldrich. The human fibroblast cell line (MRC-5, HL95001) was obtained from the Interlab Cell Line Collection (ICLC).

2.2 Measurements

The pH was measured as the change in the open circuit potential between the WE and the RE (potentiostat/galvanostat Palmsens3, Palmsens). The reference pH meter was a Crison Basic 20 with an XS Sensor glass electrode model Micro P. The temperature-resistance (T-R) curve was measured by a digital multimeter (Model 2700, Keithley), whereas the calibration was performed with a thermostatic bath (F 32, Julabo) and a temperature controller (ME, Julabo).

X-ray photoelectron spectroscopy (XPS) analysis was performed on self-standing thick films of GO and rGO directly mounted on the XPS sample holder and then installed in a (ultra-high vacuum) UHV analysis chamber. The chamber also contained a VSW-TA10 X-

ray source and a VSW-HA100 hemispherical analyser mounting a 16-channel detector, both by PSP Vacuum Technology. The X-ray non-monochromatic source (Mg Kα radiation, 1253.6 eV) was operated at 100 W (10 kV and 10 mA). The analyser was provided with a differential pumping stage to operate down to a pressure of $5 \cdot 10^{-8}$ mbar in the main chamber. XPS spectra were measured at normal emission with a fixed pass energy of 10 eV. The inelastic background in the spectra was subtracted by Shirley's method (Shirley, 1972). The deconvolution of the XPS spectra was carried out using the product of Gaussian and Lorentzian line shapes for each component and imposing an identical FWHM of about 1.3±0.1 eV. As an independent calibration was impossible due to the lack of additional reference signals, the spectra were aligned by placing the component of the C*1s* spectra corresponding to the sp^2 carbon of graphene at 284.6 eV in good agreement with earlier reports (Liu et al. 2010; Meng and Park, 2012; Stankovich et al., 2006; Stathi et al., 2015).

Micro-Raman spectroscopy was carried out using a Renishaw Raman Invia instrument. The instrument was equipped with an 1800 grooves/mm diffraction grating, a charge-coupled device (CCD) detector, a 50X magnifying lens, and a 532 nm Nd:YAG diode laser. Lorentzian fitting via the Levenberg-Marquardt algorithm was used to calculate the band peaks and the full width at half-maximum (FWHM).

A Quanta 450 FEG by FEI was used for scanning electron microscope (SEM) analysis.

2.3 GO and rGO synthesis

GO can be obtained from graphite oxide by mechanical exfoliation. We synthesized graphite oxide by Hummers' method (Hummers and Offeman, 1958) with slight

modifications to the temperature of the reactions. A solution of strong oxidizing agents was used to oxidize the graphite powder and produce graphite oxide:

$$\text{Graphite} + H_2SO_4 + NaNO_3 + KMnO_4 \rightarrow \text{Graphite Oxide}$$

In this reaction, the manganese heptoxide (Mn_2O_7), formed by the reaction of potassium permanganate ($KMnO_4$) and sulfuric acid (H_2SO_4):

$$2\ KMnO_4 + 2\ H_2SO_4 \rightarrow Mn_2O_7 + 2\ KHSO_4 + H_2O$$

is the main graphite's oxidizing reactant. Sulfuric acid, sodium nitrate and potassium permanganate were purchased from Sigma Aldrich, and the resulting GO dispersion (concentration 4 mg/mL) was used to fabricate pH sensors.

2.4 Fabrication of sensors

The pH sensing board included four working electrodes (WEs) and one reference electrode (RE). Each WE consisted of a 16 μm graphite layer (diameter 2 mm), whereas the RE was a 20 μm thick layer of Ag/AgCl (diameter 1 mm). The PET board was coated with the polyester resin to passivate the whole surface except for the active areas of the WEs and the RE. A GO dispersion (1.2 μL, concentration 4 mg/mL) was drop-casted and left to dry on each WE to obtain pH-sensitive films.

The fabrication of temperature sensors started by diluting the previous GO dispersion (concentration 0.1 mg/mL) and drop-casting 10 μL aliquots onto each of the four 6 mm x 3.5 mm temperature sensitive areas housed on a flexible PET board. Each area included a pair of screen printed silver electrodes (length 6 mm, width 600 μm, spacing 500 μm) (Fig. 1c). After drop-casting, the coated electrodes were left to dry for 6 h at room temperature and then for 1 h at 110 °C to improve the adhesion between the silver electrodes and the GO layer. The GO reduction was carried out by dipping the layer for 20 min in 200 mL of deionized water at 80 °C containing 0.5 g of ascorbic acid. Afterwards, the sensor was rinsed with deionized water and dried in an oven for 3 h at 110 °C.

2.5 Biocompatibility test

The GO and rGO biocompatibilities were investigated according to the European Union Directive 90/385/EEC. The MRC-5 cells were grown in minimum essential medium (MEM) culture with 10% FBS at 37°C in a humidified atmosphere containing 5% CO_2. Direct contact tests were performed by placing test specimens in cell culture wells. The non-cytotoxicity of the boards was assessed using the Cell Proliferation Reagent WST-1 following the protocol described by Roche Diagnostics. The specimens were placed in a broth medium that included MEM with 10% FBS and MRC-5 (p33) cells. The MRC-5 cell layer was in direct contact with 50 mm^2 specimens. Ten thousand cell/well for 96 wells were incubated for 24 h in the presence of the culture medium. As a control, some wells were used without any specimen.

The study protocol was approved by the reference Ethical Committee, protocol number DAM/MD/002/15. The research was performed in accordance with the guidelines of the Declaration of Helsinki and with informed consent from all the subjects involved.

3. Results and Discussion

3.1 XPS analysis

The efficiency of the optimized Hummers' method and the GO reduction were evaluated using the XPS analysis. A significant number of oxidized carbon groups is desirable to enhance the GO's pH sensing properties, as the amount of oxygen is directly proportional to the presence of the pH-sensitive groups such as OH, COOH and COC. Conversely, for temperature sensing, a good conductivity is only obtained if rGO mainly consists of non-

oxygenated carbons resulting from an efficient reduction and the restoration of the typical graphene sp^2 hybridization. The investigation of the C*1s* region of the GO sample and the comparison with the rGO sample analysis performed by high resolution XPS enabled the efficiency of the reduction process and the abundance of the residual functional groups in rGO to be estimated (Fig. 2).

The GO and rGO samples were prepared *ex situ*, thus an analogous analysis of the O*1s* region was not reliable due to the spurious contribution of physisorbed water.

Table 1 summarises the results of the semi-quantitative analysis performed in the C*1s* region in accordance with previous works. In agreement with the literature (Liu et al. 2010; Meng and Park, 2012; Stankovich et al., 2006; Stathi et al., 2015), the carbonylic (C=O) and epoxy and hydroxyl (C-O) species dominated the GO sample. After reduction, the main contribution to the C*1s* signal was provided by non-oxygenated carbons, however a significant fraction of oxidized carbons persisted, similarly to the other rGO systems mentioned above. The peak intensities of the oxygen-containing carbons was 87% in the GO sample and decreased to 29% after reduction (Table 1. Since the XPS penetration depth is limited to a few nanometres, this estimation only refers to the near surface layer of the sample). This decrease is close to the result (65%) reported by Akhavan *et al.* using green tea to reduce GO (Akhavan et al., 2012).

3.2 Micro-Raman spectroscopy

Fig. 3 shows the characteristic D, G, 2D and D+D' bands of the GO and rGO spectra. The D band arises from the breathing modes of the phonon dispersions near the K points in the Brillouin zone, and is activated by defects in the graphene structure, whereas the G band accounts for the E_{2_g}phonon at the Brillouin zone centre. The I_D/I_G intensity ratio of the D and G peaks depends on the defect density and can be used to estimate the mean defect

distance L_D (Grimm et al., 2016). For defective graphene, two stages can be identified according to I_D/I_G, namely stage 1, corresponding to a largely intact graphene lattice, and stage 2, corresponding to a graphene dominated by defects. In our samples, we found the D and G bands at 1350 and 1585 cm^{-1} for GO, respectively, whereas the corresponding rGO bands were at 1346 and 1585 cm^{-1}. The I_D/I_G ratios were 0.96 and 1.14 for GO and rGO, respectively. The D band FWHMs were 136 and 109 cm^{-1} for GO and rGO, respectively. The G band FWHMs were 72 and 68 cm^{-1} for GO and rGO, respectively. These results agree with those reported by (Zhang et al., 2010) and (Eigler et al., 2012) for rGO obtained by chemical reduction, e.g. using ascorbic acid or hydrazine. The I_D/I_G change after reduction depended on the removal of functional groups and the creation of defects. The D band shift and the invariance of the G band are typical of defective graphene. This result, associated with the I_D/I_G and FWHM values, indicates that our graphene belongs to stage 2, thus $L_D < 3$ nm can be estimated. The second order 2D band accounts for the resonant phonon scattering and does not depend on defects. The I_{2D}/I_G ratio decreases with an increasing number of graphene layers, whereas the D+D' band is only visible in the presence of defects. In stage 2, the 2D (centred at 2705 cm^{-1}) and D+D' (centred at 2839 and 2904 cm^{-1} for GO and rGO, respectively) bands are broad and not well-defined (inset Fig. 3) as reported by Cançado et al., 2011. For rGO, I_{2D}/I_G was 0.14, thus indicating about 4 sheets of graphene (Akhavan, 2015).

3.3 SEM analysis

The morphological properties of GO and rGO were investigated using SEM analysis. Fig. 3b shows the GO layer on a graphite WE. A moderate number of wrinkles and large surface flakes are visible and indicate a good exfoliation of graphite. The rGO dispersion

was less concentrated and deposited on a larger area than GO. The rGO surface on the PET substrate is smooth and the structure is compact with almost no wrinkles.

3.4 Temperature sensor

For our temperature sensor, we exploited the temperature dependence of conductivity in reduced graphene oxide. As reduced graphene oxide is similar to graphene (Stankovich et al., 2007), an analogous dependence of conductivity with temperature can be assumed for these materials. In the range -263.15 to -173.15 °C, the electrical carriers in graphene exhibit a near-ballistic transport, and conductivity can be assumed to be independent of temperature. At higher temperatures, conductivity variations depend on the density of carriers. At large carrier density, graphene behaves like a metal conductor, whereas at low carrier density, it exhibits a negative temperature coefficient (NTC) type dependence (Bolotin et al., 2008; Kong et al., 2012). As graphene resistivity is sensitive to the adsorption of water and oxygen molecules, we coated the rGO layer with the biomedical grade PDMS MED-6010. The temperature sensors were calibrated over the temperature range from 25 to 43 °C in human serum. The investigated temperature range can be used to discriminate between patients with normal and infected wounds (Dini et al., 2015; Grice et al., 1971), and is wide enough to perform measurements of clinical interest on human fluids such as blood, urine, exudate, and saliva. Initially, each sensor was individually calibrated due to the large variations in the baseline resistance related to the manual fabrication. However, we observed small variations in sensitivity over four different sensors, i.e. dR/dT was approximately 110 ± 10 Ω / °C, where R is the resistance and T the temperature. Fig. 4a shows the calibration curve ($R = -188.84 \cdot T + 20032$; R^2 = 0.999) for a temperature sensor after three cycles. After the three cycles, the root-mean-square error (RMSE) was about 30 Ω, which accounted for a repeatability error of about

±0.25 °C. Fig. 4b shows a measurement of a rGO sensor in human serum during a six-hour cycling test. The rGO temperature sensor had an error of 0.4 ± 0.1 °C. Although satisfactory for wound monitoring (Mehmood et al., 2015), this result could be improved as we hypothesized that the physical adsorption of liquid molecules onto the rGO layer was probably due to a poor adhesion of PDMS onto the PET substrate. Recently, an Al_2O_3 coating was proposed as a possible solution to stabilize graphene which could also be used for our rGO sensor (Sagade et al., 2015).

3.5 pH sensor

Before use, each GO pH sensor was conditioned by immersing it for 10 h in buffer solutions at pH 4, 7 and 10, respectively. The range between 4 and 10 is broad enough to cover the physiological variations of pH (Shi et al., 2015; Yan et al., 2014). For chronic wounds, the literature reports a pH interval between 6.5 and 9 (Dissemond et al., 2003; Gethin, 2007; Greener et al., 2005). Fig. 4c shows a typical calibration curve ($Voltage = -40.27 \cdot pH + 350.83$; R^2=0.994). The sensitivity was about 40 ± 4 mV/pH, calculated over five sensors. Each pH sensor had a repeatability error over three measurements for each pH value of about ± 4 mV. The five GO sensors and a Micro P glass electrode were compared over 1 week in a human serum sample (Fig. 4d). The calibration was performed in buffer solutions with the same chloride concentration (0.1 M) of human serum to prevent any interference on the RE.

The temperature was kept at 25 °C. Our tests showed that 1 week is the sensor lifetime in human serum, since the reference electrode (RE) had deteriorated probably because of biofouling. This hypothesis was supported by the fact that when the five pH sensors were taken out from the serum and immersed in a buffer solution at pH 7, they retrieved their functionality after 24 h (the difference between before and after immersion in serum was 0.1 pH units), thus excluding the occurrence of redox reaction in serum. The results

showed a good agreement with data from the glass electrode as the mean difference between pH data from the two sensors was about 0.1 ± 0.1 pH units (standard deviations for the glass electrode and GO sensor were 0.05 and 0.1 pH unit, respectively). In the range [25, 45] °C, the maximum dependence of the voltage reading from temperature was -0.5 mV/°C, which is a variation of about 0.01 pH/°C. Figure 4e shows the stability at pH 4 and 10 over 1 h test with a sampling time of 1 min. At nominal pH 4 and 10, the GO sensor returned 3.9 ± 0.1 and 10.1 ± 0.1, respectively. The hysteresis was assessed by increasing the pH from 4 to 10 and decreasing it from 10 to 4 (Fig. 4f). The maximum hysteresis error was 0.15 pH unit.

3.6 Biocompatibility

The pH and the temperature sensors were tested separately. After 24 h, the percentage of cells in the wells with the boards was within the variation range of the cell amount given from the control (Fig. 5). This is considered as a 0 grade toxicity, according to the international standard ISO 10993-5:2009 on the biological evaluation of medical devices, part 5, tests for in vitro cytotoxicity.

4. Conclusions

In this paper, we proposed an rGO-based and a GO-based pH sensor capable of monitoring temperature and pH, respectively, in contact with human serum over one week. The rGO sensor provided data in good agreement with reference sensors, and a different coating (e.g. Al_2O_3) may improve the stability and further reduce the observed deviations of 0.4 ± 0.1 °C. The rGO sensor response was highly linear (R^2 = 0.999) and the sensitivity of 110 ± 10 Ω was higher than that of average commercial thermistors in the range 25–43

°C. The GO pH sensor was linear over the pH range 4–10, had a sensitivity of 40 ± 4 mV/pH and a repeatability of ± 4 mV/pH. In the linear range, the stability error at lower and upper bounds was ± 0.1 pH units, whereas the hysteresis was 0.15 pH units. The GO pH sensor showed a comparable performance with a pH glass electrode in human serum over one week with a difference of 0.1 ± 0.1 pH units. An advantage of our solution is that a biocompatible and wearable board with temperature and pH sensors can be fabricated. This board can be used for point-of-care applications or for monitoring patients outside the hospital or specialized labs. Furthermore, the use of 2D materials would speed up the integration of sensors in flexible electronics and pave the way to mass production. For tests on patients, the board can be modified in terms of the size and number of sensors. Future work will include a reduction in the biofouling and improving the stability for longer periods than one week. An ion-selective membrane is under investigation to stabilize the RE in the presence of a variable concentration of chloride ions. In particular, we aim to monitor the wound status of patients affected by chronic wounds in real-time and while at home. Although the sensors' biocompatibility was assessed, the tolerability of the board in contact with the wound still needs to be investigated. A possible improvement for patient comfort could be to reduce the dimension of the sensors to obtain a micrometre scale.

References

1. Akhavan, O., Ghaderi, E., Hashemi, E., Rahighi, R. 2014. Nanoscale. 6(24), 14810–14819.
2. Akhavan, O., Ghaderi, E., Rahighi, R. 2012a. ACS Nano. 6(4), 2904–2916.
3. Akhavan, O., Kalaee, M., Alavi, Z.S., Ghiasi, S.M.A., Esfandiar A. 2012. Carbon. 50, 3015–3025.

4. Akhavan, O. 2015. Carbon. 81, 158–166.

5. American Diabetes Association. 2001. Diabetes Care. 24(1), 154–161.

6. Ang, P.K., Chen, W., Wee, A.T., Loh, K.P. 2008. J. Am. Chem. Soc. 130(44), 14392–14393.

7. Armstrong, D.G., Holtz-Neiderer, K., Wendel, C., Mohler, M.J., Kimbriel, H.R., Lavery, L.A. 2007. Am. J. Med. 120 (12), 1042–1046.

8. Biver, T., Criscitiello, F., Di Francesco, F., Minichino, M., Swager, T., Pucci, A. 2015. RSC Adv. 5, 65023–65029.

9. Bolotin, K.I., Sikes, K.J., Hone, J., Stormer, H.L., Kim, P. 2008. Phys. Rev. Lett. 101 (9), 096802.

10. Buckalew Jr., V.M., McCurdy, D.K., Ludwig, G.D., Chaykin, L.B., Russell Elkinton, J. 1968. Am. J. Med. 45(1), 32-42.

11. Cançado, L. G., Jorio, A., Martins Ferreira, E. H., Stavale, F., Achete, C. A., Capaz, R. B., Moutinho, M. V. O., Lombardo, A., Kulmala, T. S., Ferrari, A. C. 2011. Nano Lett. 11(8), 3190–3196.

12. Coyle, S., Lau, K.T., Moyna, N., Diamond, D., Di Francesco, F., Costanzo, D., Salvo, P., Trivella, M.G., De Rossi, D., Taccini, N., Paradiso, R., Porchet, J.A., Luprano, J., Ridolfi, A., Chuzel, C., Lanier, T., Revol–Cavalier, F., Schoumacker, S., Mourier, V., Convert, R., Chartier, L., De Moncuit, H., Bini, C. 2010. IEEE Trans. Inf. Technol. Biomed. 14 (2), 364–370.

13. Curto, V.F., Coyle, S., Byrne, R., Angelov, N., Diamond, D., Benito-Lopez, F. 2012. Sensor Actuat. B-CHEM. 175, 263–270.

14. Cutting, K.F. 2009. J. Wound Care. 18(5), 200, 202–205.

15. Dini, D., Salvo, P., Janowska, A., Di Francesco, F. & Romanelli, M. 2015. Wounds 27 (10), 274–278.

16. Dissemond, J., Witthoff, M., Brauns, T.C., Haberer, D., Goos, M. 2003. Hautarzt. 54 (10), 959–965.

17. Dong, H., Gao, W., Yan, F., Ji, H., Ju, H. 2010. Anal. Chem. 82 (13), 5511–5517.

18. Duffin, J., Philipson, E.A. 2010. Hypoventilation and hyperventilation syndromes, in: Mason, R.J., broaddus, V.C., Martin, T.R., King Jr., T.E., Schraufnagel, D.E., Murray, J.F., Nadel, J.A. (Eds.), Murray & Nadel's Textbook of Respiratory Medicine. Saunders Elsevier, Philadelphia, pp. 1859-1881.

19. Eigler, S., Dotzer, C., Hirsch, A. 2012. Carbon. 50(10), 3666−3673.

20. Eneroth, M., Larsson, J., Apelqvist. J. 1999. J. Diabetes Complications. 13 (5-6), 254–263.

21. Fang, X.-Y., Yu, X.-X., Zheng, H.-M., Jin, H.-B., Wang, L., Cao, M.-S. 2015. Phys Lett A. 379, 2245-2251.

22. Gethin, G. 2007. Wounds UK. 3 (3), 52–56.

23. Ghimenti, S., Tabucchi, S., Lomonaco, T., Di Francesco, F., Fuoco, R., Onor, M., Lenzi, S., Trivella, M.G. 2013. J. Breath. Res. 7, 017115.

24. Giuliani, A., Placidi, M., Di Francesco, F., Pucci, A. 2014. React. Funct. Polym. 76, 57–62.

25. Glibbery, A.B., Mani R. 1992. Int. J. Microcirc. Clin. Exp. 2, 109.

26. Greener, B., Hughes, AA., Bannister, NP., Douglass, J. 2005. J. Wound Care 14 (2), 59–61.

27. Grice, K., Sattar, H., Sharratt, M., Baker, H. 1971. J. Invest. Dermatol. 57, 108–110.

28. Grimm, S., Schweiger, M., Eigler, S., Zaumseil, J. 2016. J. Phys. Chem. C. 120(5), 3036–3041.

29. Health at a Glance: Europe 2010. 2010. Organisation for Economic Co-operation and Development (OECD) Publishing.

30. Hu, W., Peng, C., Luo, W., Lv, M., Li, X., Li, D., Huang, Q., Fan, C. 2010. ACS Nano. 4 (7), 4317–4323.

31. Hummers, W.S., Offeman, R.E. 1958. J. Am. Chem. Soc. 80 (6), 1339.

32. Hunt, J.F., Fang, K., Malik, R., Snyder, A., Malhotra, N., Platts-Mills, T.A., Gaston, B. 2000. Am. J. Respir. Crit. Care Med. 161 (3 Pt 1), 694–699.

33. Kleinberg, I. 1964. Arch. Oral Biol. 9(5):493-516.

34. Kong, D., Le, L.T., Li, Y., Zunino, J.L., Lee, W. 2012. Langmuir. 28 (37), 13467–13472.

35. Kraut, J.A., Kurtz I. 2005. Am. J. Kidney Dis. 45 (6). 978–993.

36. Lavery, L.A., Higgins, K.R., Lanctot, D.R., Constantinides, G.P., Zamorano, R.G., Athanasiou, K.A., Armstrong, D.G., Agrawal, C.M. 2007. Diabetes Care 30 (1), 14–20.

37. Lee, M.H., Kim, B.J., Lee, K.H., Shin, I.S., Huh, W., Cho, J.H., Kang, M.S. 2015. Nanoscale. 7(17), 7540–7544.

38. Liu, F., Seo, T. S. 2010. Adv. Funct. Mater. 20, 1930–1936.

39. Maalouf, N.M., Cameron, M.A., Moe, O.W., Adams-Huet, B., Sakhaee, K. 2007. Low Urine pH: A Novel Feature of the Metabolic Syndrome. Clin. J. Am. Soc. Nephrol. 2(5):883-888.

40. Matzeu, G., Pucci, A., Savi, S., Romanelli, M., Di Francesco, F. 2012. Sensor Actuat. A-Phys. 178, 94–99.

41. Mehmood, N., Hariz, A., Templeton, S., Voelcker, N.H. 2015. Biomed. Eng. Online. 14, 1-17.

42. Meng, L-Y., Park, S-J. 2012. Bull. Korean Chem. Soc. 33, 209–214.

43. Mueklow, J.C., Bending, M.R., Kahn, G.C., Dollery, C.T. 1978. Clin. Pharmacol. Ther. 24(5), 563-570.

44. Norn, M.S. 1988. Acta Ophthalmol. 66 (5), 485–489.

45. Osterberg, T., Landahl, S., Hedegård, B. 1984. J. Oral Rehabil. 11 (2), 157-170.

46. Remer, T., Manz, F. 1995. J. Am. Diet. Assoc. 95 (7), 791-797.

47. Sagade, A.A., Neumaier, D., Schall, D., Otto, M., Pesquera, A., Centeno, A., Zurutuza Elorza, A., Kurz, H. 2015. Nanoscale. 7, 3558–3564.

48. Salvo, P. Smajda, R., Dini, V., Saxby, C., Voirin, G., Romanelli, M., Di Francesco, F. 2016. J. Tissue Viability 25, 83–90.

49. Salvo, P., Dini, V., Di Francesco, F. & Romanelli, M. 2015a. Wound Medicine 8, 15–18.

50. Salvo, P., Melai, B., Bianchi, S., Calisi, N., Dini, V., Romanelli, M., Castelvetro, V., Paoletti, C., Politino, C., Di Francesco, F. 2015. 37th IEEE Conference of the Engineering in Medicine and Biology Society (EMBC).

51. Shao, Y., Wang, J., Wu, H., Liu, J., Aksay, I.A., Lin, Y. 2010. Electroanalysis. 22 (10), 1027–1036.

52. Shi, B., Zhang, L., Lan, C., Zhao, J., Su, Y., Zhao, S. 2015. Talanta. 142, 131–139.

53. Shih, C.J., Lin, S., Sharma, R., Strano, M.S., Blankschtein, D. 2012. Langmuir. 28 (1), 235–241.

54. Shirley, D.A. 1972. Phys. Rev. B. 5, 4709–4714.

55. Singh, N., Armstrong, D.G., Lipsky, B.A. 2005. JAMA 293(2), 217–228.

56. Stankovich, S., Dikin, D.A., Piner, R.D., Kohlhaas, K.A, Kleinhammes, A., Jia, Y., Wu, Y., Nguyen, S.T. 2007. Carbon. 45 (7), 1558–1565.

57. Stankovich, S., Piner, R.D., Chen, X., Wu, N., Nguyen, S.T., Ruoff, R.S. 2006. J. Mater. Chem. 16 (2), 155–158.

58. Stathi, P., Gournis, D., Deligiannakis, Y., Rudolf, P. 2015. Langmuir. 31 (38), 10508–10516.

59. Taniguchi, T., Kurihara, S., Tateishi, H., Hatakeyama, K., Koinuma, M., Yokoi, H., Hara, M., Ishikawa, H., Matsumoto, Y. 2015. Carbon. 84 (1), 560–566.

Figure1

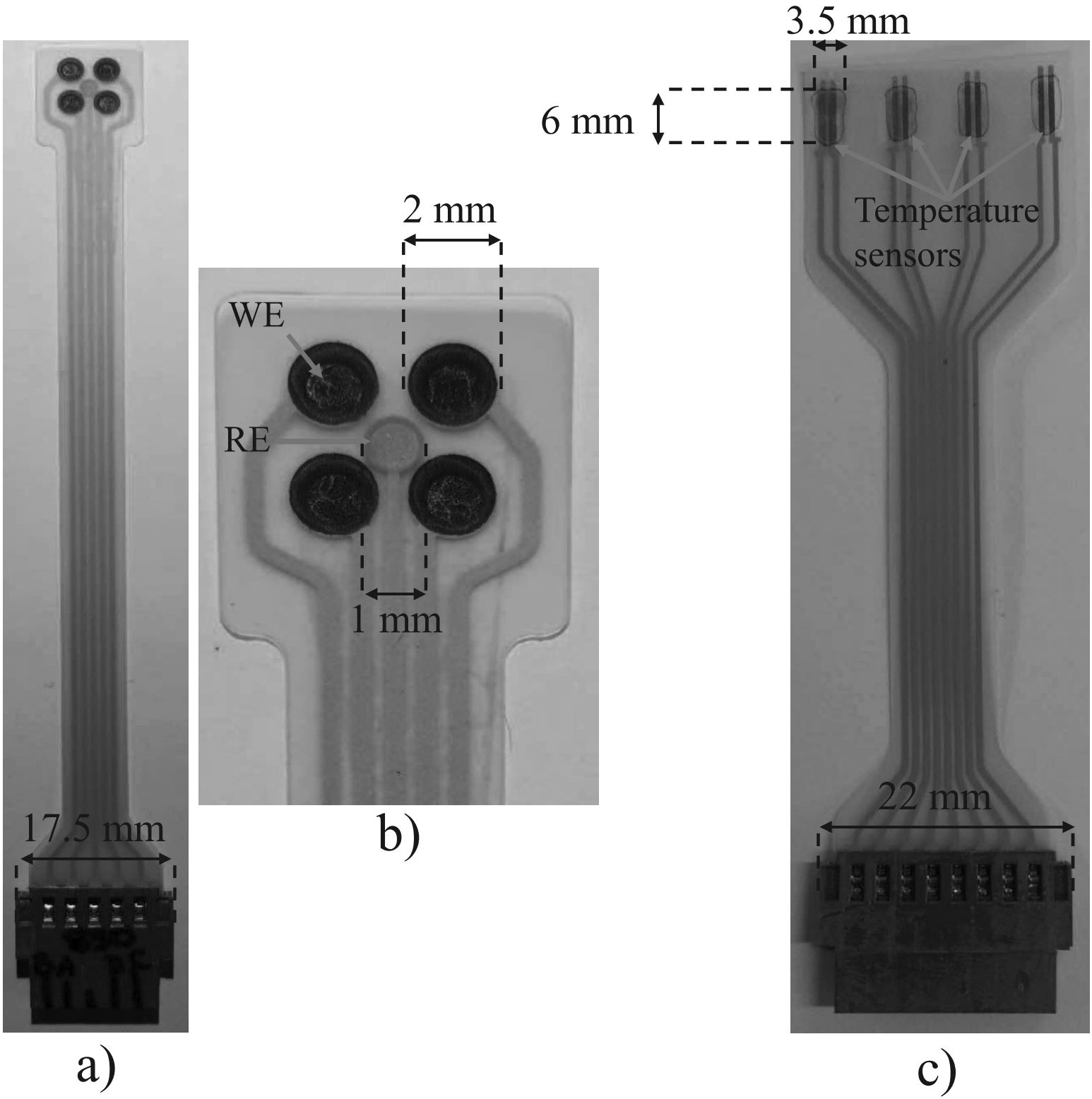

Figure2

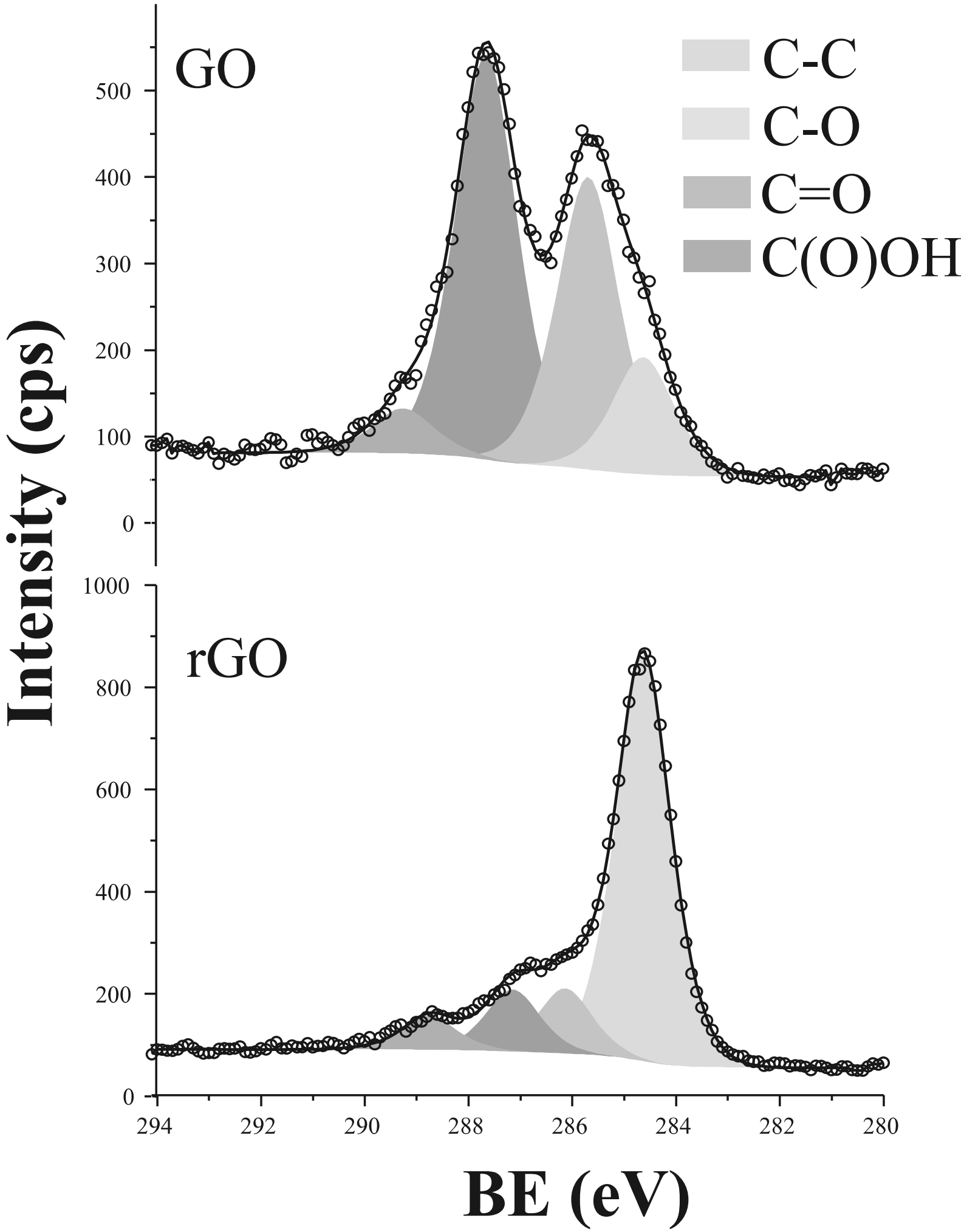
GO
C-C
C-O
C=O
C(O)OH
rGO
Intensity (cps)
BE (eV)
0
100
200
300
400
500
0
200
400
600
800
1000
294
292
290
288
286
284
282
280

Figure3

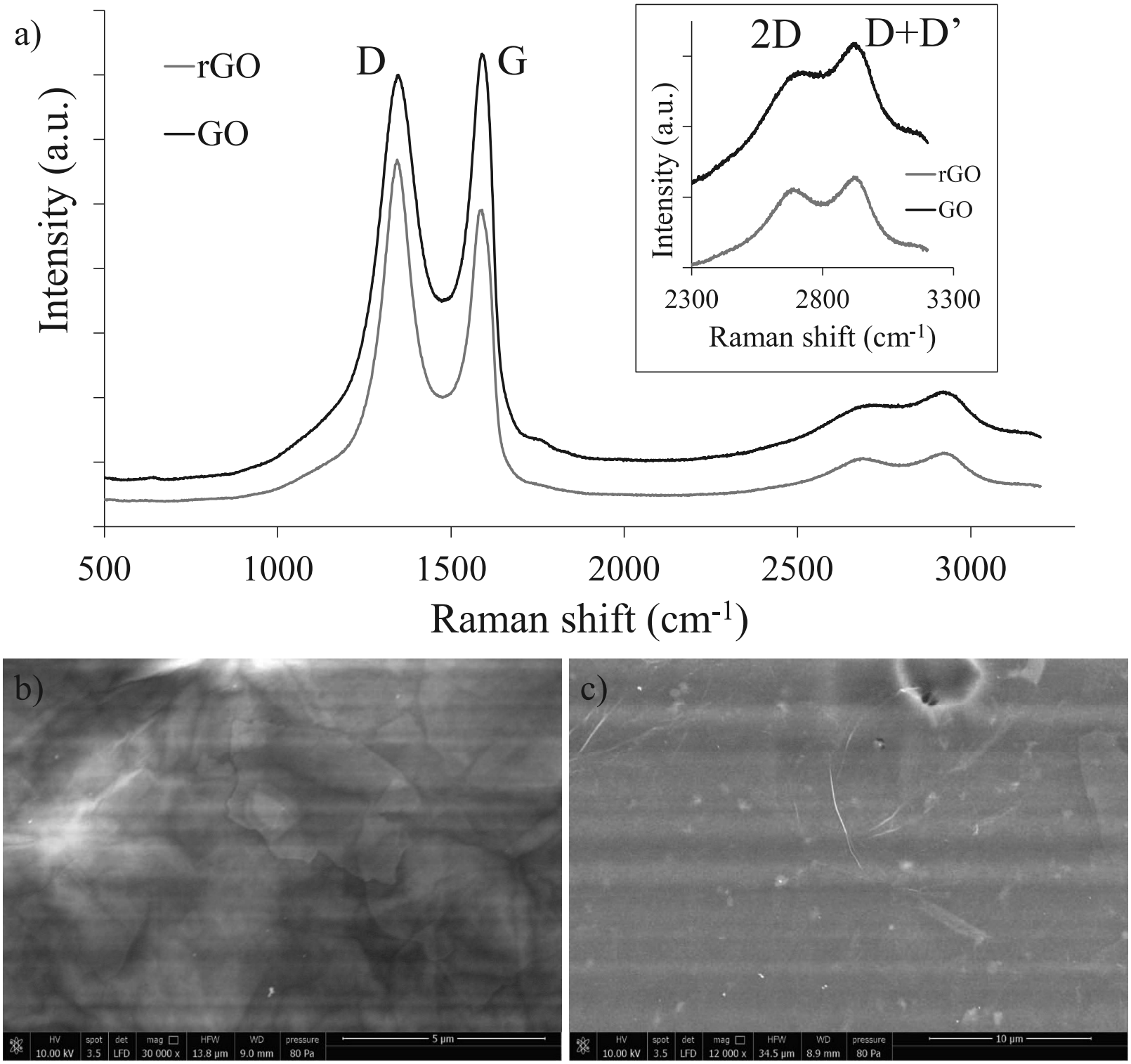
a)
rGO
GO
D
G
Intensity (a.u.)
500
1000
1500
2000
2500
3000
Raman shift (cm-1)
2D
D+D'
Intensity (a.u.)
rGO
GO
2300
2800
3300
Raman shift (cm-1)
b)
HV 10.00 kV
spot 3.5
det LFD
mag 30 000 x
HFW 13.8 µm
WD 9.0 mm
pressure 80 Pa
5 µm
c)
HV 10.00 kV
spot 3.5
det LFD
mag 12 000 x
HFW 34.5 µm
WD 8.9 mm
pressure 80 Pa
10 µm

Figure4

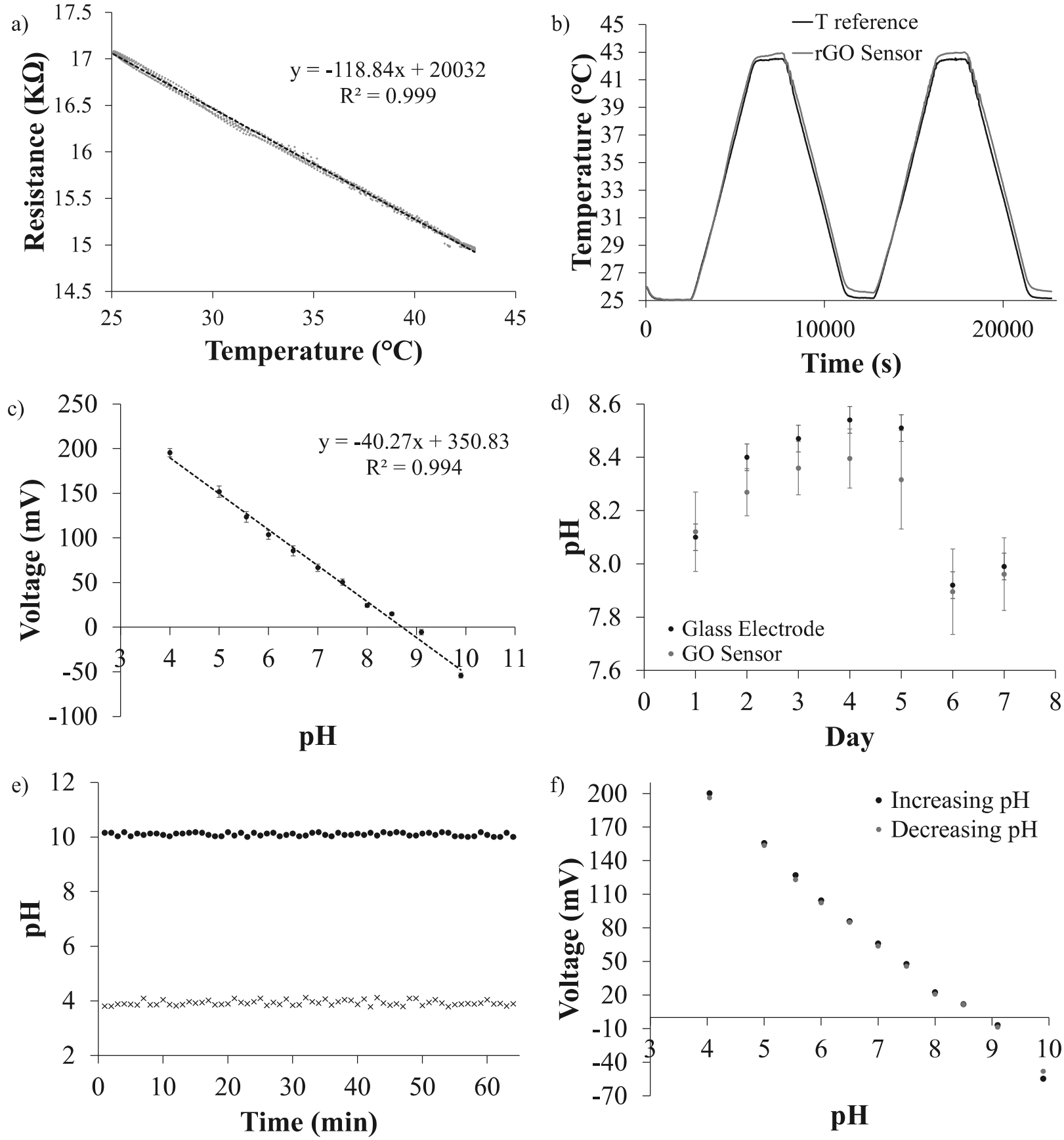
a)
y = -118.84x + 20032
R² = 0.999
Resistance (KΩ)
Temperature (°C)
b)
T reference
rGO Sensor
Temperature (°C)
Time (s)
c)
y = -40.27x + 350.83
R² = 0.994
Voltage (mV)
pH
d)
Glass Electrode
GO Sensor
pH
Day
e)
pH
Time (min)
f)
Increasing pH
Decreasing pH
Voltage (mV)
pH

Figure5

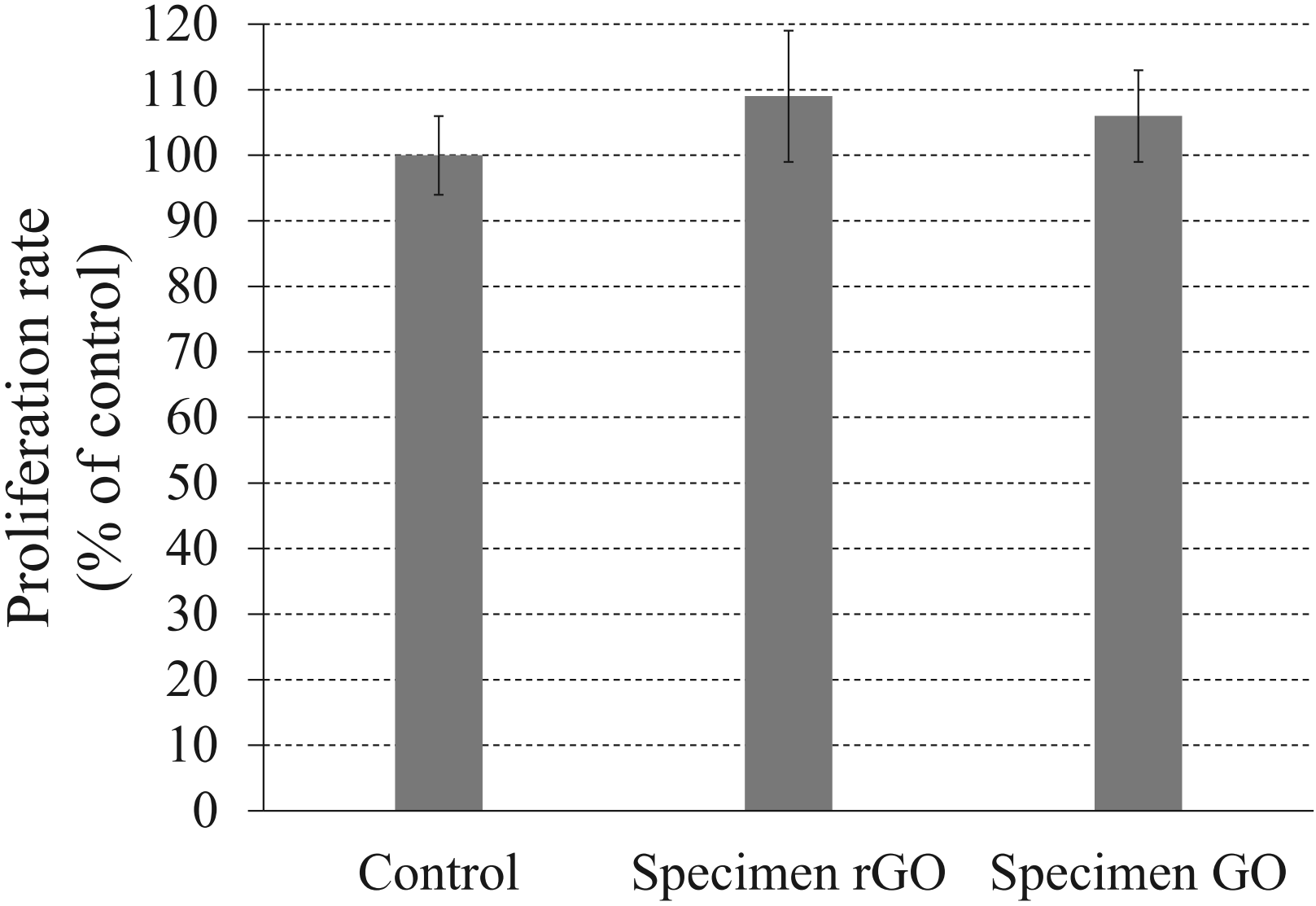
Proliferation rate
(% of control)
120
110
100
90
80
70
60
50
40
30
20
10
0
Control
Specimen rGO
Specimen GO

Tables

Table 1. Functional group percentages in the GO and rGO samples and total O-containing carbons resulting from the deconvolution of the XPS spectra. The binding energies (BE) were estimated with reference to the sp^2 carbon of graphene as described in the methods.

	GO [BE (eV)]	rGO [BE (eV)]
C-C	13% [284.6]	71% [284.6]
C-O	34% [285.7]	12% [286.1]
C=O	47% [287.6]	11% [287.1]
C(O)OH	6% [289.2]	6% [288.7]
O-containing C	87%	29%